An Experimental Investigation of Cusped Magnetic Field Discharge Chambers

John R. Brophy* and Paul J. Wilbur†
Colorado State University, Fort Collins, Colorado

Several features of a proposed model of ion thruster performance are tested experimentally. Experiments demonstrate the effects of variation in thruster geometry and operating parameters on the average plasma ion energy cost and extracted ion fraction. Results indicate that the model correctly predicts the variation in the plasma ion energy cost resulting from changes in propellant flow rate, propellant utilization efficiency, propellant gas, grid system transparency to neutral atoms, beam extraction area, and discharge voltage. Results suggest that to use the proposed thruster performance model as an aid in thruster design, the four thruster configuration/propellant dependent parameters—C_0, ϵ_P^*, f_B, and f_C—may be taken to be independent of the propellant utilization efficiency and flow rate. At low discharge voltages, however, this simple formulation begins to break down. The discharge voltage at which this occurs is dependent on the propellant gas.

Introduction

THIS paper describes experiments performed to test the validity of several features of the thruster performance model developed in the preceding article.[1] Specifically, measurements of the plasma ion energy cost ϵ_P were made as a function of the neutral density parameter $\dot{m}(1-\eta_u)$ and are compared to the predictions of the model as given by

$$\epsilon_P = \epsilon_P^* [1 - \exp\{-C_0 \dot{m}(1-\eta_u)\}]^{-1} \quad (1)$$

where C_0 is the primary electron utilization factor, ϵ_P^* the baseline plasma ion energy cost, $\dot{m}$ the propellant flow rate in units of equivalent amperes (A eq), and η_u the propellant utilization efficiency. These experiments were conducted on argon and krypton propellant gases, and the effects of variations in propellant flow rate, propellant utilization efficiency, discharge voltage, grid system transparency to neutral atoms, and beam extraction area were examined. In addition, the extracted ion fraction f_B, defined as the ratio of beam current to total ion current produced, was measured over this same range of operating parameters. Tests were performed on both ring and line cusp thruster geometries.

Experimental Apparatus

The ion source shown schematically in Fig. 1 was designed and built for this investigation. This source normally produces a 12-cm diam ion beam and provides the capability for measuring the distribution of ion currents to the beam, screen grid, and all internal thruster surfaces except the anode and the cathode wires and support posts.

The magnetic field for this experimental ion source is established through the use of an electromagnet located on the upstream centerline of the discharge chamber and a number of 1.9 cm × 1.3 cm × 0.5 cm samarium cobalt permanent magnets. These permanent magnets are arranged end-to-end to form ring magnets of alternate polarity in the manner suggested by Fig. 1. The flux density at the surface of the magnets is 0.27 T and the magnets are attached to the steel discharge chamber housing by their own magnetic attraction. This arrangement allows the ion source magnetic field configuration to be altered quickly and easily by simply adding, removing, or changing the position of the magnets. For the configuration shown in Fig. 1, the upstream magnet ring is covered with a strip of 0.13 mm thick steel insulated from the magnets themselves by a strip of 0.25 mm thick flexible mica. This is done so that this surface can be maintained at anode potential while the rest of the thruster body is biased negative of cathode potential. The downstream magnet ring is uncovered. The magnetic flux density at the surface of the electromagnet can be adjusted from 0 to approximately 0.2 T by adjusting the magnet current from 0 to 124 A.

The main discharge chamber cathode consists of seven 0.25-mm-diam tungsten wires connected in parallel and supported by two support posts that are electrically isolated from the thruster body. Each cathode wire is approximately 2.8 cm long, so the total cathode emission length exposed to the plasma is about 19.6 cm. These seven short wires in parallel are used to minimize the voltage drop across the cathode. A voltage drop of less than 3 V at the maximum heater current used was achieved with this system. It is noted that a small voltage drop across the cathode results in a primary electron energy distribution that more closely resembles the monoenergetic distribution produced by a hollow cathode. The cathode wires were heated using direct currents in the range 6 to 8 A per wire. Tests were conducted using both argon and krypton propellants. Discharge voltages were varied from 30 to 50 V for argon and 20 to 40 V for krypton. The discharge current was adjusted through the range of 0.5 to 5 A for both propellants by controlling the heater current through the refractory cathode wires.

Two ion accelerator systems were used in this study. The first accelerator system consisted of a set of dished, small-hole accelerator grids (SHAG) with a cold grid separation of 0.75 mm and screen and accelerator grid physical open-area fractions of 0.68 and 0.30, respectively. The second system consisted of a set of dished, large-hole accelerator grids (LHAG) with a cold grid separation of 0.75 mm, and screen and accelerator grid physical open-area fractions of 0.68 and 0.57, respectively. Both accelerator systems were normally masked to produce a 12-cm-diam beam. One series of tests was conducted, however, with the SHAG set masked to produce a 6-cm-diam beam. For the 12-cm-diam beam tests, flow rates for both argon and krypton were varied from 500 to 1500 mA eq. For the 6-cm-diam beam test, the flow rates were varied from 125 to 500 mA eq. All tests were conducted in a 1.2-m-diam × 4.6-m-long vacuum test facility. Tank pressures ranged from approximately 2×10^{-6} Torr with no

Received Aug. 1, 1984; revision submitted Feb. 11, 1985.

*Research Assistant, Department of Mechanical Engineering; presently at the Jet Propulsion Laboratory, Pasadena, CA. Member AIAA.

†Professor, Department of Mechanical Engineering. Member AIAA.

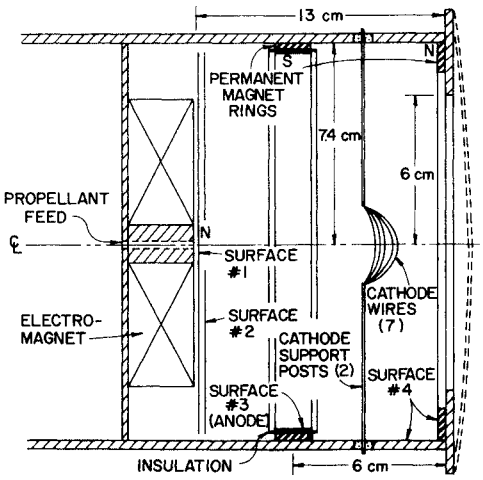

Fig. 1 Ring cusp ion thruster schematic.

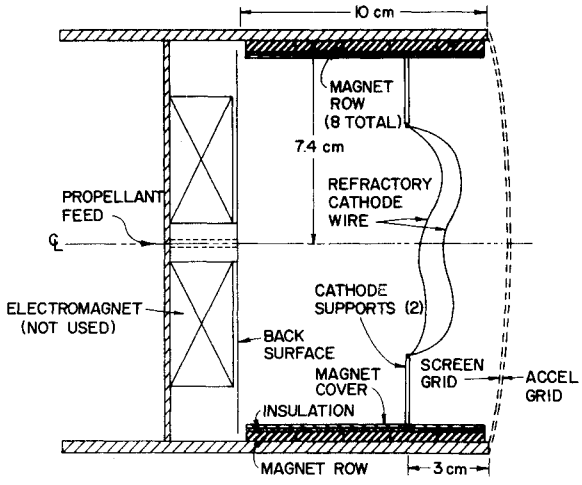

Fig. 2 Line cusp ion thruster schematic.

flow to approximately 3×10^{-5} Torr at a flow rate of 1500 mA eq.

A second series of tests were performed on the line cusp thruster configuration shown schematically in Fig. 2. The magnetic field for the configuration is established using eight rows of samarium cobalt permanent magnets of alternating polarity positioned along the cylindrical discharge chamber side wall. Six of the magnetic rows were maintained at anode potential, while the other two (diametrically opposite) rows were biased negative of cathode potential along with the back surface, side wall, and screen grid. Tests were conducted over a range of argon propellant flow rates of 600 to 1600 mA eq, discharge voltages of 40 to 50 V, and discharge currents of 0.5 to 4.0 A. The current through the electromagnet was maintained at zero for these tests.

Procedure

The following set of experiments was designed to test the suitability of the model just described to predict the functional dependence of the parameter ϵ_p on the neutral density parameter $\dot{m}(1-\eta_u)$. The model pedicts that the plasma ion energy cost should behave according to Eq. (1). The value of ϵ_p may be determined experimentally through the use of the equation

$$\epsilon_p = [J_D - (J_C + J_B)]/J_P \tag{2}$$

where J_D is the discharge current, J_C the ion current to cathode potential surfaces, J_B the beam current, and J_P the total ion production current. Note that the power used to operate the thermionic cathodes is not included in Eq. (2). In order to use Eq. (2) one must be able to measure each of the parameters on the right-hand side of the equation. Measurement of the discharge current, discharge voltage, and beam current is straightforward. To measure the ion currents J_C and J_P, the thruster configuration of Fig. 1 was operated with only the upstream magnet ring at anode potential. All other interior discharge chamber surfaces (with the exception of the cathode support posts) were biased approximately 30 V negative of cathode potential to repel the discharge chamber electrons. At this bias the current to these surfaces consists only of the incoming ion current. If the ion current to the cathode supports posts and cathode wires is neglected—which is permissible since the area of these surfaces is relatively small—then the ion current measured in the manner described above is equal to J_C.

To determine J_P, it is noted that the total ion production current may be given as the sum of the ion currents leaving the plasma, i.e.,

$$J_P = J_B + J_C + J_A \tag{3}$$

where J_A is the ion current to anode potential surfaces. Since the anode is exposed to the plasma only at a magnetic field cusp, the effective area for ion loss to this surface is expected to be less than the physical area.[3-6] Rough calculations indicate that the ion current to the anode with this configuration should be less than a few percent of the total production current. Thus, J_P may be approximated as the sum of the ion currents to the beam (including the impingement current) and to the negatively biased discharge chamber surfaces (including the screen grid).

Complete sets of data consisting of the beam current, propellant flow rate, propellant utilization, and total ion production current were collected over the range of operating conditions discussed earlier with the electromagnetic current held constant at 57 A for the ring cusp thruster and at zero for the line cusp thruster. At each condition tested, the thruster was operated at flow rates of 500, 750, 1000, and 1500 mA eq. At each flow rate, the discharge voltage was held constant, while the discharge current was varied. Increasing the discharge current increased the beam current and propellant utilization, thus decreasing the neutral density parameter $\dot{m}(1-\eta_u)$. By operating in this manner, the full range of neutral density parameters from close to zero to nearly 1500 mA eq could be investigated. Thus, the plasma ion energy cost was determined from Eq. (2) for a wide range of operating conditions. The extracted ion fraction f_B, defined by

$$f_B = J_B/J_P \tag{4}$$

was also measured over this same range of conditions.

Results and Discussion

Plasma Ion Energy Cost

Measurement of the plasma ion energy cost for operation of the ring cusp thruster with argon propellant at a 50-V discharge over the range of neutral flow rates from 500 to 1500 mA eq yielded the results shown in Fig. 3. Here the measured values of the energy cost of a plasma ion ϵ_P are plotted as a function of the neutral density parameter $\dot{m}(1-\eta_u)$ associated by Eq. (1). The solid line in Fig. 3 is the curve given by Eq. (1), when the parameters C_0 and ϵ_P have been selected to give the best fit to the data. The parameter ϵ_P^* was taken to be the value of ϵ_P measured at large values of the neutral density parameter. The reason for this can be understood by considering Eq. (1), which shows that when $C_0\dot{m}(1-\eta_u)$ is large, the exponential term is small compared to unity and one obtains $\epsilon_P = \epsilon_P^*$. Having established

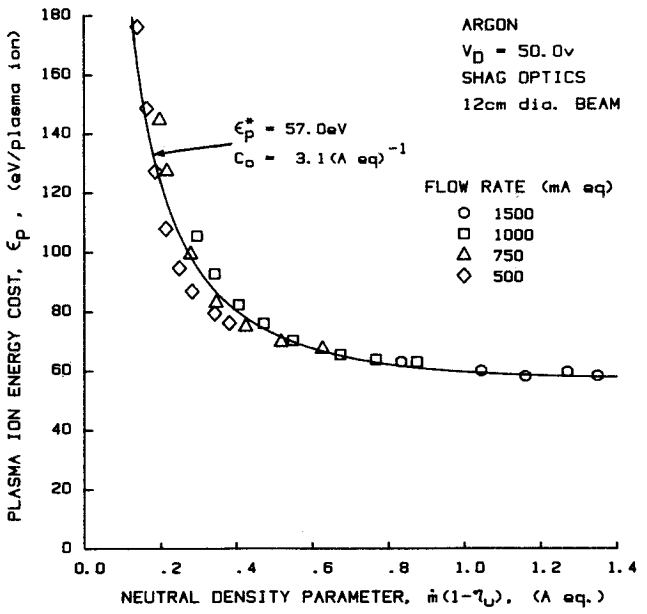

Fig. 3 Reference plasma ion energy cost curve.

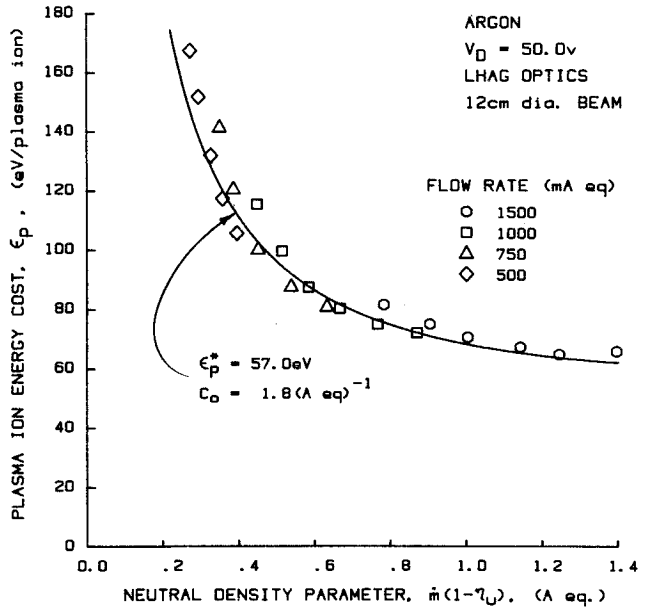

Fig. 4 Plasma ion energy cost curve for high accelerator grid transparency.

the value of the baseline plasma ion energy cost, the value of the primary electron utilization factor C_0 is varied until the best fit is obtained. The agreement between the functional form of Eq. (1) and the experimental data is seen to be quite good. This indicates that the parameters C_0 and ϵ_P^* may be taken to be independent of the neutral density parameter.

A value of $C_0 = 3.1$ (A eq)$^{-1}$, which is applicable to the ion source of Fig. 1 operating at the conditions defined in the legend for Fig. 3, has now been established. New values of the primary electron utilization factor applicable to other operating conditions may be calculated from this value using the definition of C_0

$$C_0 = 4\sigma_0 \ell_e / e v_0 A_g \phi_0 \tag{5}$$

For example, changing grid sets from SHAG to LHAG should change the value of C_0 through the parameter ϕ_0, which is the effective transparency of the grids to neutral atoms. This effective transparency parameter may be calculated for each grid set, according to the equation

$$\phi_0 = \phi_s \phi_a / (\phi_s + \phi_a) \tag{6}$$

where ϕ_s and ϕ_a are the modified transparencies for the screen and accelerator grids, respectively. The modified transparency may be calculated as the physical open-area fraction of a grid times the appropriate Clausing factor.[7] For the two grid sets used in this study,

$$\phi_{0_{\mathrm{SHAG}}} = 0.16, \quad \phi_{0_{\mathrm{LHAG}}} = 0.27 \tag{7}$$

Thus, the new value of the primary electron utilization factor applicable to the LHAG optics with all other conditions held constant is given by,

$$(C_0)_{\mathrm{new}} = \frac{\phi_{0_{\mathrm{SHAG}}}}{\phi_{0_{\mathrm{LHAG}}}} (C_0)_{\mathrm{Fig.\ 3}} \tag{8}$$

which yields $(C_0)_{\mathrm{new}} = 1.8$ (A eq)$^{-1}$.

The measured values of ϵ_P obtained under the same set of conditions defined in the legend of Fig. 3, except for the change in optics from SHAG to LHAG, yielded the results shown by the data points in Fig. 4. The solid line is the prediction of the model based on the value of C_0 calculated from Eq. (8). The value of the baseline plasma ion energy cost was held constant at $\epsilon_P^* = 57$ eV since changing the optics should not affect this parameter. The degree of agreement between the data points and the curve in Fig. 4 shows clearly that the model correctly predicts the variation in the plasma ion energy cost with the neutral density parameter when the grid system transparency to neutrals is changed.

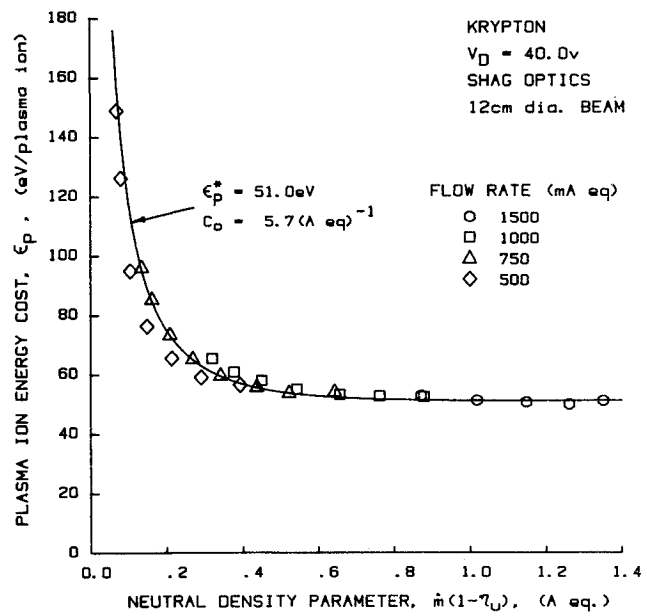

Fig. 5 Plasma ion energy cost curve for krypton.

The same procedure of calculating a new value of the primary electron utilization factor from the old value according to Eq. (5) was followed for the analysis of the data displayed in Figs. 5 through 8. For the data in Fig. 5, the thruster was operated with krypton propellant and SHAG optics at a discharge voltage of 40 V. The primary electron utilization factor corresponding to this operating condition was calculated using the value of C_0 obtained from Fig. 3, together with Eq. (3) in the form

$$(C_0)_{\mathrm{new}} = \frac{(\sigma_0)_{\mathrm{kr}}}{(\sigma_0)_{\mathrm{Ar}}} \frac{m_{\mathrm{kr}}}{m_{\mathrm{Ar}}} (C_0)_{\mathrm{Fig.\ 3}} \tag{9}$$

In this case, both the change in propellant properties and the change in discharge voltage must be accounted for. That is,

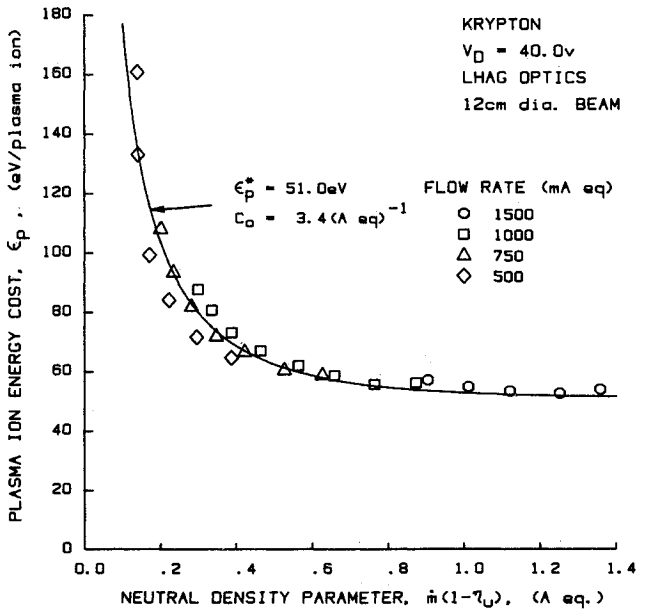

Fig. 6 Plasma ion energy cost curve for krypton and a high accelerator grid transparency.

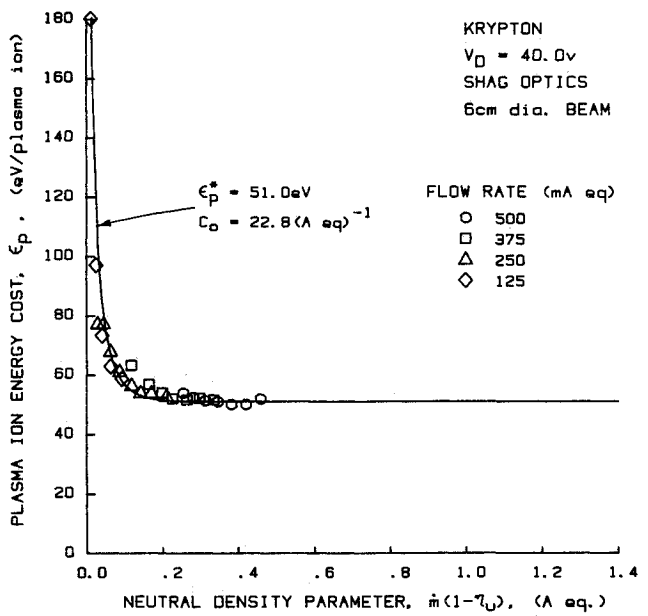

Fig. 7 Plasma ion energy cost curve for a small-diameter ion beam.

$(\sigma_0)_{kr}$ is the total inelastic collision cross section for 40-eV primary electron/krypton atom collisions, whereas $(\sigma_0)_{Ar}$ refers, in this case, to 50-eV primary electron/argon atom collisions. The cross-section data needed in this equation were obtained from de Heer et al.[8] The new value of the primary electron utilization factor calculated from Eq. (9) was $C_0 = 5.7$ (A eq)$^{-1}$, and the corresponding prediction of the model is compared to the measured values in Fig. 5. A new value of the baseline plasma ion energy cost ϵ_p^* was also required to fit the data of Fig. 5, since this parameter should be a function of both the discharge voltage and the propellant type. This new value was selected in the manner suggested previously as the measured plasma ion energy cost at high neutral density levels. Results similar to those of Fig. 5, showing that the model correctly describes the performance on xenon propellants, are presented in Ref. 2.

Continuing the procedure of predicting a new primary electron utilization factor using the model and comparing the model prediction to the experimental results yields the comparison of Fig. 6 for operation with LHAG optics, krypton propellant, and $V_D = 40$ V. Again, the agreement between the predicted curve and the experimental data is seen to be good.

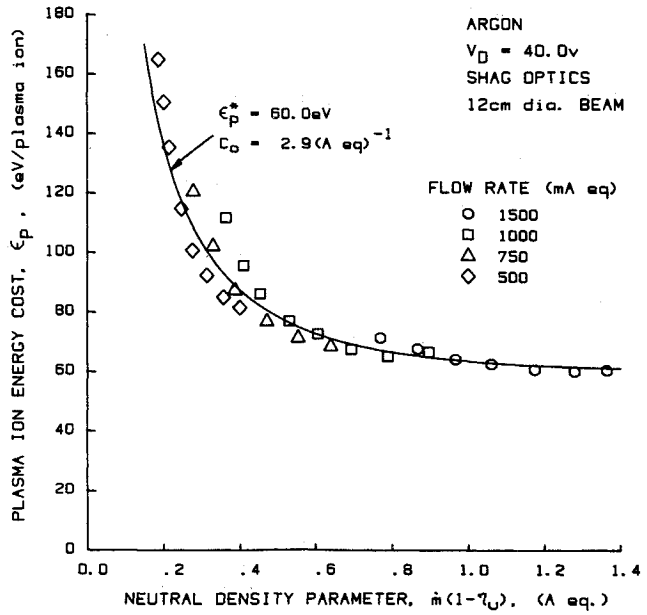

Fig. 8 Plasma ion energy cost curve for 40-V argon discharge.

From Eq. (5) it is seen that the primary electron utilization factor depends inversely on the area of the grids through which the beam is extracted, A_g. This area may be varied without changing the discharge chamber diameter by masking down the screen grid to produce ion beams of different cross-sectional areas. In this case, the screen grid for the SHAG optics set was masked down from a beam diameter of 12 cm to one of 6 cm. This fourfold reduction in beam area should produce a corresponding fourfold increase in the primary electron utilization factor. Taking C_0 for Fig. 4 and multiplying by four yields the new value of $C_0 = 22.8$ (A eq)$^{-1}$. The model prediction for the plasma ion energy cost vs neutral density parameter curve obtained using this value of C_0 is compared to the measured values of these quantities in Fig. 7. Remarkably, the agreement between the model and the experiment is excellent. Similar agreement was obtained for operation with argon using the masked-down grid set.

Next, the dependency of the plasma ion energy cost on discharge voltage for a given propellant is investigated. For operation with argon at $V_D = 40$ V, a new value of the primary electron utilization factor was calculated from the value given in Fig. 3, which was based on a discharge voltage of 50 V. Again the model agrees well with the measured values as shown in Fig. 8, provided a new value of the baseline plasma ion energy cost of 60 eV is used.

For operation at a 30-V discharge voltage with argon, however, the situation is quite different, as seen in Fig. 9. Here a systematic difference in the data taken at different flow rates is observed. Clearly a single equation such as Eq. (1) is not sufficient to explain this behavior if C_0 and ϵ_p^* are taken to be independent of the neutral flow rate and the propellant utilization. Expressing the neutral density parameter as $\dot{m} - J_B$ suggests that a given value of this parameter obtained at different propellant flow rates corresponds to different beam currents. Further, the different beam currents may be roughly translated into different plasma densities. Thus, a possible theoretical interpretation of the data in Fig. 9 might be found by looking for the primary electron utilization factor and/or the baseline plasma ion energy cost to be functions of the plasma density at low discharge voltages.

For krypton propellant, this separation with flow rate was found to occur at a discharge voltage of ~20 V rather than

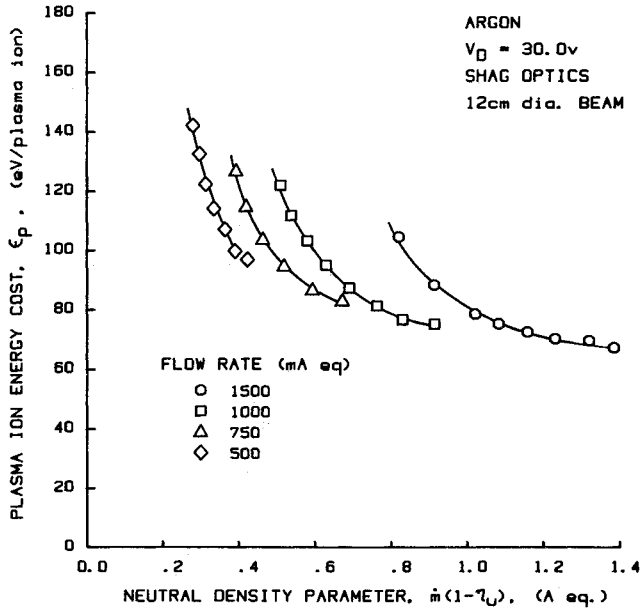

Fig. 9 Plasma ion energy cost curve for 30-V argon discharge.

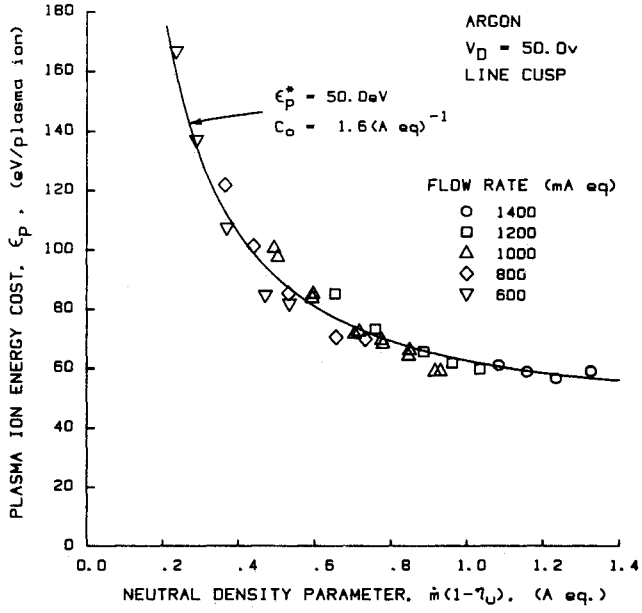

Fig. 10 Plasma ion energy cost curve for line cusp configuration.

the ~30 V value observed for argon. This indicates that the separation phenomenon depends on the properties of the ions (or neutrals) in the discharge chamber as well as the discharge voltage.

Experiments performed on the line cusp configuration of Fig. 2 indicated that the model is applicable to line cusp as well as ring cusp thruster designs. An example of the results obtained with the line cusp discharge chamber is given in Fig. 10 for operation with argon propellant at a discharge voltage of 50 V. Good agreement between the model and the experiment is obtained for values of $C_0 = 1.6$ (A eq)$^{-1}$ and $\epsilon_P^* = 50$ eV.

Extracted Ion Fraction

Aside from the plasma ion energy cost, the other parameter that has a major effect on thruster performance is the extracted ion fraction f_B. It is of little use to create ions efficiently in the discharge chamber if the fraction of these ions extracted into the beam is small. The extracted ion fraction, which is defined as the beam current divided by total

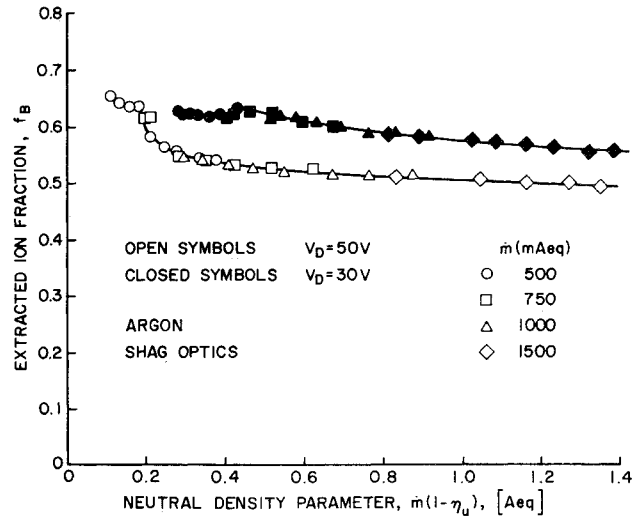

Fig. 11 Extracted ion fraction results.

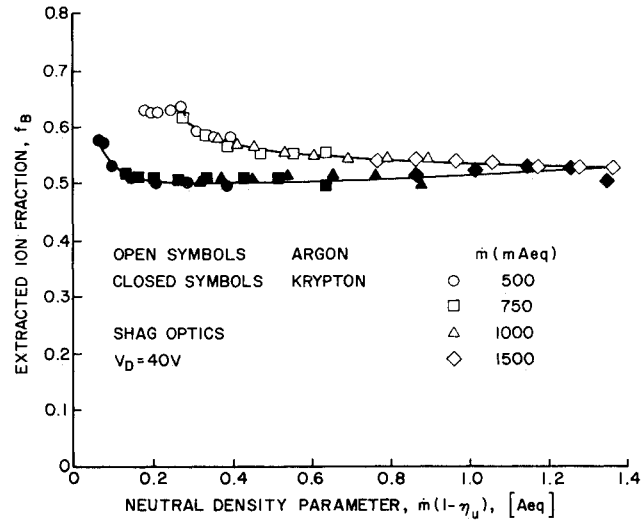

Fig. 12 Extracted ion fraction results.

ion production current [Eq. (4)], was measured over the same set of operating conditions described earlier. The resulting extracted ion fraction data were found to correlate poorly with the propellant utilization, where a systematic difference between data taken at different flow rates was observed for all cases. The extracted ion fraction data were found, however, to correlate well with the neutral density parameter. The reason for this correlation is not known. In any case, the data will be presented here as a function of this parameter, as shown in Fig. 11.

In this figure, values of f_B are given for operation with argon propellant at discharge voltages of both 30 and 50 V over a range of flow rates from 500 to 1500 mA eq. Several things are evident from these data. First, the degree of correlation for the data taken at different flow rates and a fixed discharge voltage is quite good. Second, the extracted ion fraction is greater at the lower discharge voltage. These conclusions were found to be true for all sets of data taken. The data taken under the same conditions but at a 40-V discharge voltage fall between the two curves shown in Fig. 11. Third, f_b is seen to increase slightly with decreasing values of the neutral density parameter. Finally, it is noted that the extracted ion fraction data in Fig. 11 taken at a 30-V discharge voltage still correlate well with the neutral density parameter at this low discharge voltage, even if the corresponding plasma ion energy cost data of Fig. 9 did not.

The extracted ion fractions for argon propellant are compared to those for krypton at a discharge voltage of 40 V in

Fig. 12. The values of f_B for argon are seen to be generally higher than those for krypton.

It should be pointed out that none of the effects exhibited in Figs. 11 and 12 are understood at this time. Earlier studies indicate that the extracted ion fraction is strongly dependent on the magnetic field configuration.[9,10] However, since it is not a strong function of the neutral density parameter, increasing only slightly with decreasing values of this parameter, a simple design approach would be to take f_B to be a constant for a given discharge chamber design (magnetic field configuration), propellant, and discharge voltage.

Conclusions

Several features of a proposed model of ion thruster operation have been tested experimentally. The model predicts the functional dependence of the plasma ion energy cost on the neutral density parameter $\dot{m}(1-\eta_u)$. Experiments indicate good agreement between the predicted functional form of the model and the experimental data. These data also suggest that the primary electron utilization factor C_0 and baseline plasma ion energy cost are relatively independent of the neutral density parameter.

The model correctly predicts the variation in plasma ion energy cost for changes in propellant gas, grid transparency to neutrals, beam extration area, and discharge voltage. In addition, the model is shown to be applicable to both ring and line cusp thruster designs.

Measurements of the extracted ion fraction indicate that this parameter correlates well with the neutral density parameter, although the physical basis for this correlation is not understood. The extracted ion fraction tends to increase with decreasing discharge voltage and tends to increase for operation with argon as opposed to krypton propellant.

To use the proposed model for design purposes, it is suggested, on the basis of the results in this paper, that the parameters C_0, ϵ_P^*, f_B, and f_C be taken to be constants for a given thruster design. That is, these parameters should be taken to be independent of the neutral density parameter, and dependent only on the thruster geometry, magnetic field configuration, propellant gas, and discharge voltage. Comparison of thruster design for operation at the same discharge voltage and propellant gas would eliminate the last two parameters from consideration.

For operation at low discharge voltages the simple model with C_0 and ϵ_P^* as constants begins to break down. The discharge voltages at which this occurs depends on the propellant gas. For argon this occurred at a discharge voltage of around 30 V, for krypton it was closer to 20 V.

Acknowledgment

This work performed under NASA Grant NGR-06-002-112.

References

[1]Brophy, J. R. and Wilbur, P. J., "Simple Performance Model for Ring and Line Cusp Ion Thrusters," *AIAA Journal*, Vol. 23, Nov. 1985, pp. 1731-1736.

[2]Brophy, J. R., "Ion Thruster Performance Model," NASA CR-174810, Dec. 1984.

[3]Hershkowitz, N., Leung, K. N., and Romesser, T., "Plasma Leakage Through a Low-β Line Cusp," *Physical Review Letters*, Vol. 35, No. 5, 1975, pp. 277-280.

[4]Leung, K. N., Hershkowitz, N., and Mackenzie, K. R., "Plasma Confinement by Localized Cusps," *The Physics of Fluids*, Vol. 19, No. 7, 1976, pp. 1045-1053.

[5]Hershkowitz, N., Smith, J. R., and Kozima, H., "Electrostatic Self-Plugging of a Picket Fence Cusped Magnetic Field," *Physics of Fluids*, Vol. 22, No. 1, 1979, pp. 122-125.

[6]Kozima, H., Kawamoto, S., and Yamagiwa, K., "On the Leak Width of Line and Point Cusp Magnetic Fields," *Physics Letters*, Vol. 86A, No. 6,7, 1981, pp. 373-375.

[7]Clausing, P., "Über die Stromung Sehr Verdünnter Gase Durch Rören von Beliebiger Länge," *Annalen der Physik*, Vol. 12, 1932, pp. 961-989.

[8]de Heer, F. J., Jansen, R.H.J., and van der Kaay, W., "Total Cross Sections for Electron Scattering by Ne, Ar, Kr, and Xe," *Journal of Physics B: Atomic, Molecular Physics*, Vol. 12, No. 6, 1979, pp. 979-1002.

[9]Brophy, J. R. and Wilbur, P. J., "The Flexible Magnetic Field Thruster," *Journal of Spacecraft and Rockets*, Vol. 20, Nov-Dec. 1983, pp. 611-618.

[10]Brophy, J. R. and Wilbur, P. J., "Recent Developments in Ion Sources for Space Propulsion," *Proceedings of the Ion Engineering Congress—ISIAT '83 and IPAT '83*, Kyoto, Japan, 1983, pp. 411-422.